Phosphonic Acid Functionalized Periodic Mesoporous Organosilicas and Their Potential Applications in Selective Enrichment of Phosphopeptides

ARTICLE *in* THE JOURNAL OF PHYSICAL CHEMISTRY C · FEBRUARY 2009

Impact Factor: 4.77 · DOI: 10.1021/jp8093534

8 AUTHORS, INCLUDING:

Hua Zhong
Micromeritics China
12 PUBLICATIONS **281** CITATIONS

SEE PROFILE

THE JOURNAL OF PHYSICAL CHEMISTRY C

Article

Phosphonic Acid Functionalized Periodic Mesoporous Organosilicas and Their Potential Applications in Selective Enrichment of Phosphopeptides

Peiyuan Wang, Liang Zhao, Ren'an Wu, Hua Zhong, Hanfa Zou, Jie Yang, and Qihua Yang

J. Phys. Chem. C, **2009**, 113 (4), 1359-1366• DOI: 10.1021/jp8093534 • Publication Date (Web): 06 January 2009

Phosphonic Acid Functionalized Periodic Mesoporous Organosilicas and Their Potential Applications in Selective Enrichment of Phosphopeptides

Peiyuan Wang,[†,‡,¶] Liang Zhao,[‡,§,¶] Ren'an Wu,[*,§] Hua Zhong,[†,‡] Hanfa Zou,[§] Jie Yang,[†] and Qihua Yang[*,†]

State Key Laboratory of Catalysis, Dalian Institute of Chemical Physics, Chinese Academy of Sciences, 457 Zhongshan Road, Dalian 116023, People's Republic of China, Graduate School of the Chinese Academy of Sciences, Beijing 100049, People's Republic of China, and National Chromatographic R&A Center, Dalian Institute of Chemical Physics, Chinese Academy of Sciences, 457 Zhongshan Road, Dalian 116023, People's Republic of China

Received: October 22, 2008; Revised Manuscript Received: December 02, 2008

Phosphonic acid functionalized periodic mesoporous organosilicas were synthesized by co-condensation of 1,2-bis(trimethoxysilyl)ethane and diethoxyphosphorylethyl-triethoxysilane in acidic medium using Brij-76 as a template. Structural characterizations showed that the mesoporous materials with 2-D hexagonal mesostructures could be obtained in the presence of an inorganic salt, NaCl. The results of transmission electron microscopy revealed that the materials synthesized with NaCl/Brij-76 mass ratios of 3 and 4 had extensive structural defect holes in the nanochannels. After coordinating metal ions (Zr^{4+} and Fe^{3+}) with phosphonic acid in the mesopore, the materials were applied as the potential immobilized metal affinity chromatographic adsorbent for the selective enrichment of phosphopeptides. Because of the stronger affinity interaction between the coordinated metal ions and the phosphoryl groups of phosphopeptides, the higher surface area, and the unique mesoporous structure, the capture of the phosphopeptide on the phosphonic acid functionalized periodic mesoporous organosilicas were much more efficient than that on the commercial POROS-20 beads.

1. Introduction

The reversible phosphorylation of proteins is recognized as an essential post-translational modification regulating cell signaling and ultimate functions of biological systems.[1] The mass spectrometry-based methods for detecting and mapping phosphorylation have paved the way for understanding complex biological processes. The minimal amount of phosphorylated proteins in biological systems and the serious ion suppression phenomenon arising from the proteolytic complexity in mass spectrometry have been quite a challenge for the analysis of phosphoproteins.[2] The selective capture of phosphopeptides from complex proteolytic products would provide a great opportunity for circumventing the difficulties in the analysis of phosphoproteins. Various materials, such as agarose, beaded cellulose, and porous silica have been used as adsorbents in immobilized metal affinity chromatography (IMAC).[3,4] In comparison with materials mentioned above, mesoporous silicas with high surface area, large pore volume, and ordered pore structure may be interesting adsorbents in IMAC. However, the low stability of mesoporous silicas under strong acid or basic conditions inhibits their application in the enrichment of phosphopeptides because the phosphopeptides are loaded at low pH and the captured phosphopeptides are eluted at high pH.

Since the recent emergence of periodic mesoporous organosilicas (PMOs) synthesized from $(R'O)_3Si\text{-}R\text{-}Si(OR')_3$,[5−7] PMOs have garnered much research attention due to the unique properties derived from the combination of highly ordered mesostructures and the bridged organic groups uniformly distributed in the framework, which endow them powerful properties with potential applications in adsorption, separation, catalysis, photonics, quantum dots, etc.[8−17] Unlike the mesoporous silicas functionalized with the organic groups obtained via grafting or co-condensation methods, the PMOs with organic groups covalently bonded and homogeneously distributed in the framework can give rise to great possibilities for tuning the chemical and physical properties of PMOs in designated ways by varying the structure and chemical compositions of the precursors. The majority of the organic groups in the framework of PMOs were based upon short aliphatic (methane, ethane, ethene) or rigid aromatic (phenylene, thiophene) groups.[9,10,12,15] To expand the materials' composition and add doped functional components, the bifunctionalized PMOs (BPMOs) with much wider application potentials than PMOs were synthesized by introducing the organic groups both in the framework and in the pore of the PMOs via co-condensation of $(R'O)_3SiRSi(OR')_3$ and $(R'O)_3SiR$.[18−27]

Because of the presence of bridged organic groups in the framework, PMOs demonstrate higher stability in a wide pH range than conventional mesoporous silicas.[6,28] A previously synthesized phenyl-functionalized mesoporous ethane silica has been used as a stable packing material for high performance liquid chromatography under a strong basic medium (pH = 10).[29] For taking the unique advantages of BPMOs, the phosphonic acid functionalized PMOs were successfully synthesized in this work via the co-condensation of 1,2-bis(tri-

* To whom correspondence should be addressed. E-mail: yangqh@dicp.ac.cn (Q.H.Y.); wurenan@dicp.ac.cn (R.A.W.). Phone: 86-411-84379552; 86-411-84379576. Fax: 86-411-84694447; 86-411-84379620.

† State Key Laboratory of Catalysis, Dalian Institute of Chemical Physics, Chinese Academy of Sciences.

‡ Graduate School of the Chinese Academy of Sciences.

§ National Chromatographic R&A Center, Dalian Institute of Chemical Physics, Chinese Academy of Sciences.

¶ These authors contributed equally to this work.

10.1021/jp8093534 CCC: $40.75
Published on Web 01/06/2009

SCHEME 1: Synthesis of Phosphonate Ester and Phosphonic Acid Functionalized Mesoporous Organosilica

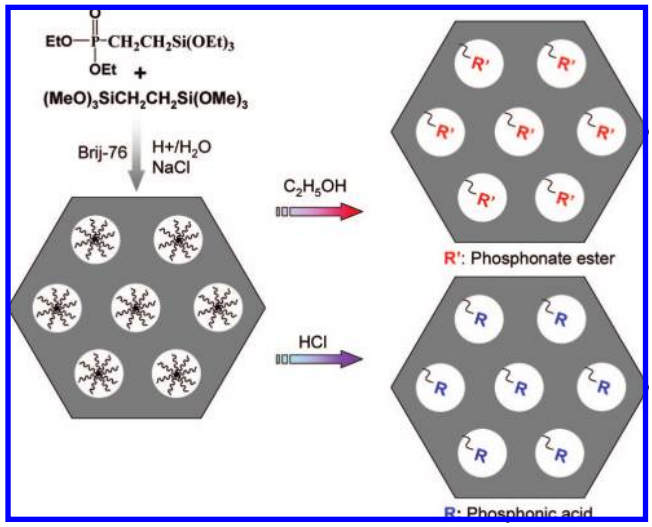

methoxysilyl)ethane (BTME) and diethoxyphosphorylethyltriethoxysilane (PETES) under acidic medium using Brij-76 as a template. The phosphonic groups in the BPMOs could be utilized as suitable coordination sites for immobilizing metal ions (Zr^{4+} and Fe^{3+}) and would be applied as the potential affinity material for the specific capture of phosphorylated peptides.[30−36] The obtained BPMOs were systematically characterized by X-ray diffraction (XRD), transmission electron microscopy (TEM), nitrogen adsorption, and NMR and were examined by matrix-assisted laser desoprtion−ionization time-of-flight mass spectrometry (MALDI-TOF MS) for the specific enrichment of phosphopeptides from a tryptic digest of bovine β-casein based on the preload of metal ions (Zr^{4+} and Fe^{3+}).

2. Experimental Section

2.1. Chemicals and Reagents. BTME, β-casein (from bovine milk), $C_{18}H_{37}(OCH_2CH_2)_{10}OH$ (Brij-76), trypsin, 2,5-dihydroxybenzoic acid (2,5-DHB), and zirconium oxychloride ($ZrOCl_2 \cdot 8H_2O$) were purchased from Sigma-Aldrich Company, Ltd. (USA). PETES was from Gelest, Inc. (Germany). Ammonium bicarbonate, dithiothreitol (DTT), and iodoacetamide (IAA) were purchased from BioRad (Hercules, CA, USA). Acetonitrile (ACN), ethanol, and trifluoroacetic acid (TFA) were purchased from Merck (Darmstadt, Germany). Water used in all experiments was doubly distilled and purified by a Milli-Q system (Millipore, Milford, MA, USA). Other reagents were purchased from ShangHai Chemical Reagent. Inc. of Chinese Medicine Group. All materials were of analytical grade and used as purchased without further purification.

2.2. Synthesis of Phosphonic Acid Functionalized Mesoporous Organosilicas (EPO-*m*). In a typical synthesis process, Brij-76 (2.0 g) was dissolved in HCl solution (32 g, 2 M) and H_2O (16 g) at 55 °C under vigorous stirring. A mixture of BTME and PETES was added to the above solution, and the resulting mixture was stirred at 55 °C for 36 h. The solid product was recovered by filtration and air-dried at room temperature overnight. The molar ratio of the original gel was 1.00 Si/0.141 Brij-76/3.20 HCl/127 H_2O. The as-synthesized material was refluxed in concentrated HCl (50 mL, 36.5 wt %) at 100 °C for 24 h. The powder product was filtered and washed with large amounts of deionized water and dried at 100 °C. The obtained sample was denoted as EPO-*m*, where *m* (*m* = 0, 10, 20) is the mol % of PETES/(PETES + BTME) in the initial gel mixture.

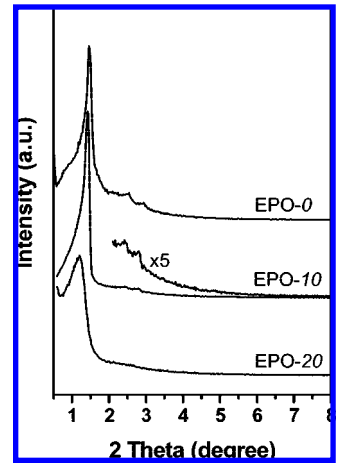

Figure 1. Powder XRD patterns of phosphonic acid functionalized mesoporous ethane silicas.

To improve the mesostructure's order, the mesoporous organosilicas were also synthesized in the presence of an inorganic salt, NaCl. The synthesis procedure was similar to that for the preparation of EPO-*m* except the addition of NaCl in the solution of Brij-76 and HCl at 55 °C, and the resulting sample was denoted as EPO-*m*-*n*, where *m* (*m* = 10, 20) is the mol % of PETES/(PETES + BTME) in the initial gel mixture and *n* (*n* = 1, 2, 3, 4) is mass ratio of NaCl/Brij-76.

To investigate the influence of surfactant extraction method on the structural properties of the material, the phosphonate ester functionalized mesoporous ethane silicas, EPO-*ma*-*n*, were obtained by refluxing 0.5 g of as-synthesized materials in 100 mL of ethanol for 24 h.

2.3. Characterizations. XRD patterns were recorded on a Rigaku RINT D/Max-2500 powder diffraction system using Cu Kα radiation. The nitrogen sorption experiments were performed at −196 °C on an ASAP 2020 system. The samples were outgassed at 120 °C for 5 h before the measurements. The Brunauer−Emmett−Teller (BET) surface area was evaluated from data in the relative pressure range from 0.05 to 0.25. The total pore volumes were estimated from the amount adsorbed at a relative pressure of 0.99. Pore diameters were determined from the adsorption branch using the Barrett−Joyner−Halenda (BJH) method. TEM was performed using a JEOL JEM-2010 at an acceleration voltage of 120 kV. ^{13}C (100.5 MHz) cross-polarization magic-angle spinning (CP-MAS) and ^{31}P (161.8 MHz) and ^{29}Si (79.4 MHz) MAS solid-state NMR experiments were recorded on a Varian infinity-plus 400 spectrometer equipped with a magic-angle spin probe in a 4-mm ZrO_2 rotor. ^{13}C and ^{29}Si signals were referenced to tetramethylsilane, and the ^{31}P NMR signal was referenced to H_3PO_4 (85 wt %). The experimental parameters were 8-kHz spin rate, 3-s pulse delay, 4-min contact time, 1500−3000 scans for ^{13}C CP-MAS NMR experiments; 4-kHz spin rate, 180-s pulse delay, 10-min contact time, 116 scans for ^{29}Si MAS NMR experiments; 10-kHz spin rate, 3-s pulse delay, 200 scans for ^{31}P MAS NMR experiments.

A MALDI-TOF mass spectrometer was used to investigate the affinity of metal ions (Zr^{4+} and Fe^{3+}) immobilized on phosphonic acid functionalized PMOs to the phosphopeptides. All MS spectra were acquired by a Bruker Autoflex time-of-flight mass spectrometer (Bruker, Bremen, Germany) equipped with a delayed ion-extraction device and a 337-nm pulsed nitrogen laser. The range of laser energy was adjusted to slightly above the threshold for obtaining good resolution and signal-to-noise ratio. All measurements were carried out by the linear

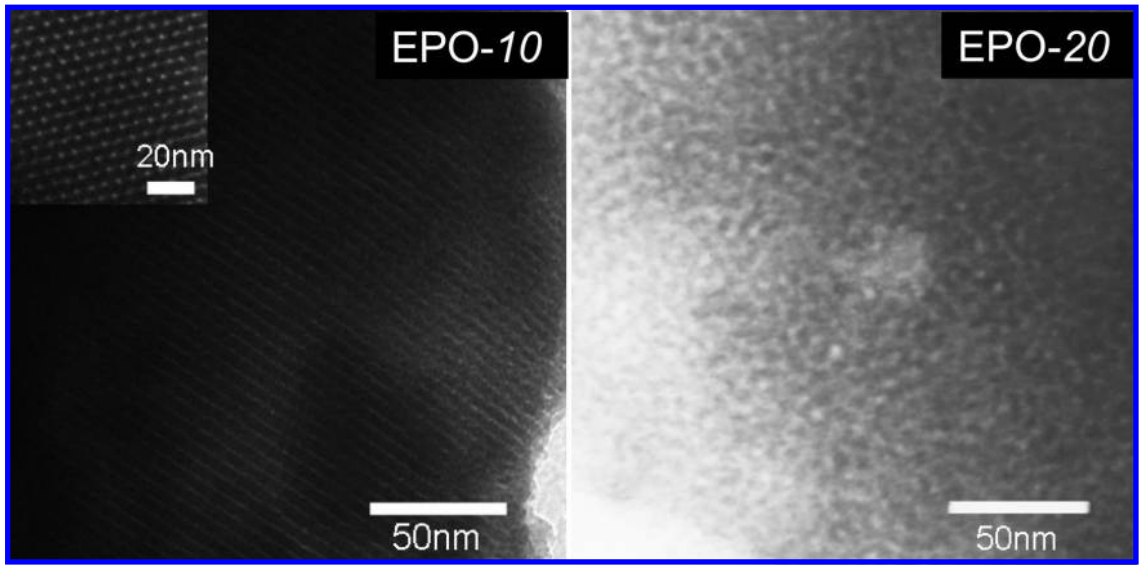

Figure 2. TEM images of EPO-10 and EPO-20.

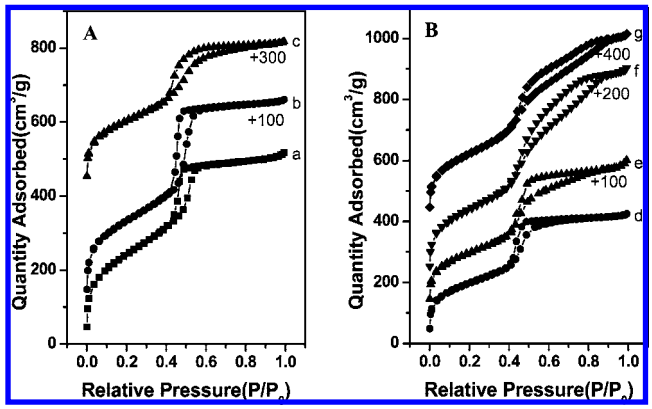

Figure 3. N_2 sorption isotherms of EPO-*m* (A) synthesized with different molar ratio of PETES/(PETES+BTME) and EPO-*m*-*n* (B) synthesized with different amount of NaCl: (a) EPO-0; (b) EPO-10; (c) EPO-20; (d) EPO-20-1; (e) EPO-20-2; (f) EPO-20-3; (g) EPO-20-4.

positive-ion mode with delayed ion extraction of 90 ns delay time and 20 kV extraction voltage. Each MS spectrum was acquired by the accumulation of 30 laser shots. For capturing phosphopeptides, the phosphonic acid-functionalized PMOs were preloaded with metal ions (Zr^{4+} and Fe^{3+}) and incubated with tryptic digests of β-casein at room temperature. After that, the captured phosphopeptides were analyzed by MALDI-TOF MS based on a series of elution, drying and preparation steps. (See Supporting Information for the details of tryptic digestion of protein and the capture of phosphopeptides.)

3. Results and Discussion

3.1. Synthesis. Phosphonate ester functionalized mesoporous organosilicas EPO-*m* were prepared by co-condensation of BTME and PETES in acidic medium using Brij-76 as a structure-directing agent. Phosphonic acid functionalities can be generated by dealkylation of phosphonate ester groups by refluxing the sample in concentrated HCl.[37] Therefore, we tried to combine the dealkylation together with the surfactant-extraction process by refluxing the as-synthesized materials in concentrated HCl. By use of this method, we may not only avoid the tedious surfactant-extraction process but also modify the textural properties of the materials. The detailed synthetic process is shown in Scheme 1.

Figure 1 shows XRD patterns of phosphonic acid functionalized mesoporous ethane silicas. Sample EPO-0 synthesized without PETES displays three well-resolved diffraction peaks with *d* spacing at 6.0, 3.5, and 3.0 nm, which can be readily indexed to the (100), (110), and (200) diffraction peaks of a 2-D hexagonal (*P6mm*) phase, respectively. Sample EPO-10 synthesized with 10% molar ratio of PETES also displays three well-resolved diffraction peaks with *d* spacings of 6.2, 3.9, and 3.1 nm, showing that EPO-10 also has ordered hexagonal mesostructure. When the molar ratio of PETES was increased to 20%, EPO-20 only displays one peak together with a broad shoulder at low diffraction angle in the XRD pattern. Such a diffraction pattern is often observed for typical disordered MSU-X materials with wormholelike structures. TEM images further confirm that EPO-10 and EPO-20 have ordered 2-D hexagonal mesostructure and wormholelike mesostructure, respectively (Figure 2).

The N_2 sorption isotherms of all EPO-*m* samples exhibit type IV isotherm pattern (Figure 3A). The H1 hysteresis loops with sharp capillary condensation step in the relative pressure P/P_0 of 0.40−0.55 were clearly observed in the N_2 sorption isotherm of EPO-0 and EPO-10, suggesting that these two materials have cylindrical pores and uniform pore size distributions (Figure S1 of Supporting Information). The hysteresis loop for EPO-20 becomes H2, and the capillary condensation step of EPO-20 is not as steep as that of EPO-0 and EPO-10. The results of N_2 sorption isotherm are consistent with the XRD results that the mesostructural order is impaired for material synthesized at high concentration of PETES. The materials have a BET surface area of 875−718 m^2/g, a pore volume of 0.8−0.65 cm^3/g, and a pore diameter of 3.8−3.5 nm (Table 1).

3.2. Effects of Inorganic Salts on the Mesostructure of the Organosilicas. The structural characterization shows that EPO-20 has disordered mesostructure. The deterioration of mesostructural ordering with the increase of PETES content is a common phenomenon for mesoporous hybrid materials synthesized by co-condensation of $RSi(OR')_3$ and $Si(OR')_4$.[21,24−27,38−41] This may be due to the weakened interactions between organosilane and Brij-76 micelles with the increase of PETES. Also, the flexibility of PETES will render the framework less rigid and lower the pore regularity. Inorganic salts have been widely used to assist the formation of highly ordered mesoporous silica templated by nonionic templates through affecting the organiza-

TABLE 1: Physicochemical Properties of Phosphonate Ester and Phosphonic Acid Functionalized Mesoporous Organosilicas

sample	*d* spacing (nm)	BET surface area (m^2 g^{-1})	pore volume (cm^3 g^{-1})	pore diameter[a] (nm)	wall thickness[b] (nm)
EPO-0	6.0	875	0.80	3.8	3.1
EPO-10	6.2	840	0.87	3.5	3.7
EPO-20	7.3	718	0.65	3.6	
EPO-20-1	6.3	703	0.66	3.2	4.1
EPO-20-2	6.1	704	0.77	3.2	3.8
EPO-20-3	6.0	867	1.09	3.2	3.7
EPO-20-4	5.8	802	0.95	3.2	3.5
EPO-20a-2	5.7	805	0.76	3.0	3.6

[a] Calculated using the BJH model on the adsorption branch of the isotherm. [b] Calculated by a_0 − pore diameter, where $a_0 = 2d_{100}/\sqrt{3}$.

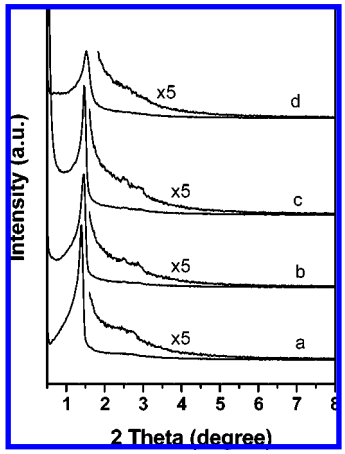

Figure 4. XRD patterns of EPO-20-*n* synthesized with different amounts of NaCl: (a) EPO-20-1; (b) EPO-20-2; (c) EPO-20-3; (d) EPO-20-4.

tion behavior of the template molecules or increasing the interactions between silica and nonionic templates.[19,20,42−46] Recently, our group reported that ordered mesoporous ethane silicas could be even synthesized at neutral conditions using Brij-76 as a surfactant with the aid of inorganic salts.[47] To improve the structural order of the material with higher amounts of phosphonic acid groups incorporated in the mesopore, the materials were synthesized with the addition of NaCl because inorganic salts are believed to play an important role in the mesosturcture formation of the surfactant-organosilica nanocomposites.

The synthesis conditions for EPO-20-*n* samples were similar to those for EPO-20 with the exception that different amounts of NaCl were added. Figure 4 shows the XRD patterns of EPO-20-*n* synthesized in the presence of different amounts of NaCl. EPO-20-1 synthesized with NaCl/Brij-76 mass ratio of 1 displays one sharp (100) diffraction peak together with a weak (200) peak in the low 2θ region. In comparison with EPO-20, the structural order of EPO-20-1 was greatly improved and *d* spacings were reduced from 7.3 to 6.3 nm due to the existence of NaCl. With a further increase in the mass ratio of NaCl/Brij-76 to 2, the XRD pattern of EPO-20-2 displays three diffraction peaks with *d* spacings of 6.1, 3.6, and 3.1 nm. To confirm the mesostructure of EPO-20-2, the TEM technique was used. The TEM images of EPO-20-*n* are shown in Figure 5. EPO-20-2 clearly shows the parallel channels of the typical two-dimensional hexagonal structures, which confirms that EPO-20-2 has 2-D hexagonal *P6mm* structure. The XRD pattern of EPO-20-3 was similar to that of EPO-20-2. The parallel fringe structure with an incidence direction perpendicular to the pore axis channels was clearly observed in the TEM image of EPO-20-3, which shows that a highly ordered 2-D hexagonal mesostructure was obtained too. It is worth noting that there are irregularly shaped holes scattered throughout the channels of EPO-20-3, showing that void defects are formed in the mesoporous framework. The existence of void defects in the pore wall of mesoporous materials connected the long linear channels and will facilitate the mass transfer of guest molecules through the porous matrix. Only one diffraction peak with decreased intensity was observed in the XRD pattern of EPO-20-4, indicating the deterioration of ordered mesoporous assembly probably as a result of too much more addition of NaCl.[48]

Similar to EPO-20-3, TEM images of EPO-20-4 also show parallel fringes with large numbers of irregularly shaped holes in the pore walls. However, the wormlike disordered mesostructure coexists, which shows that the structural order of EPO-20-4 decreased compared with EPO-20-3. The results of TEM images indicate that NaCl can favor the formation of ordered pore structure and irregularly shaped holes in the pore wall of the materials. However, the addition of large amounts of NaCl could lead to the deterioration of the ordered structure.

Under acidic conditions, an anion-mediated assembly is proposed (S^0H^+)(X^-I^+), where S^0, X^-, and I^+ are the nonionic surfactant, halide anion, and protonated Si-OH moieties, respectively. For mesoporous silica synthesized with $C_m(EO)_n$ as a template, the assembly process is driven by the interactions between the hydrophilic EO chain of $C_m(EO)_n$ and the silica oligomers. The organosilica oligomers will accumulate at the interface and coassemble with the micelles of the surfactant to form rodlike hybrid nanocomposites. When the concentration of PETES is increased up to 20 mol %, the ordered assembly will be decreased because PETES has fewer hydrolytic Si-OR groups and larger terminal bonded organic groups than BTME. When NaCl was added, Na^+ could make the hydrophilic headgroup of the surfactant more rigid and confer more positive charge to it, which will enhance the interactions between the organosilica oligomers and surfactant micelles.[47,49] In consideration of the salting-out effect of NaCl, addition of NaCl will cause the dehydration of the ethylene oxide units of Brij-76, which can render the PEO chains less hydrophilic. This will benefit the interactions between the PEO corona and the hydrophobic organosilica oligomer. Also, the addition of NaCl will lower the solubility of Brij-76 surfactant and thus reduce the critical micelle concentration (CMC).

The decrease in CMC favors the micelle−micelle interaction and enhances the assembly ability of the micelles to help the formation of the ordered phase.[47] Therefore, with the addition of appropriate amounts of inorganic salt (NaCl/Brij-76 = 2), highly ordered mesoporous materials (EPO-20-2) can be obtained. It is also known that electrolytes can modify the rate and extent of silicon alkoxide hydrolysis and condensation.[50] Strongly ionizing anions such as F^-, Cl^-, and NO_3^- increase the rate of silicate hydrolysis and condensation.[51] The presence of large amounts of Cl^- will make the hydrolysis and condensation rate of the organosilane precursor too fast, which may not

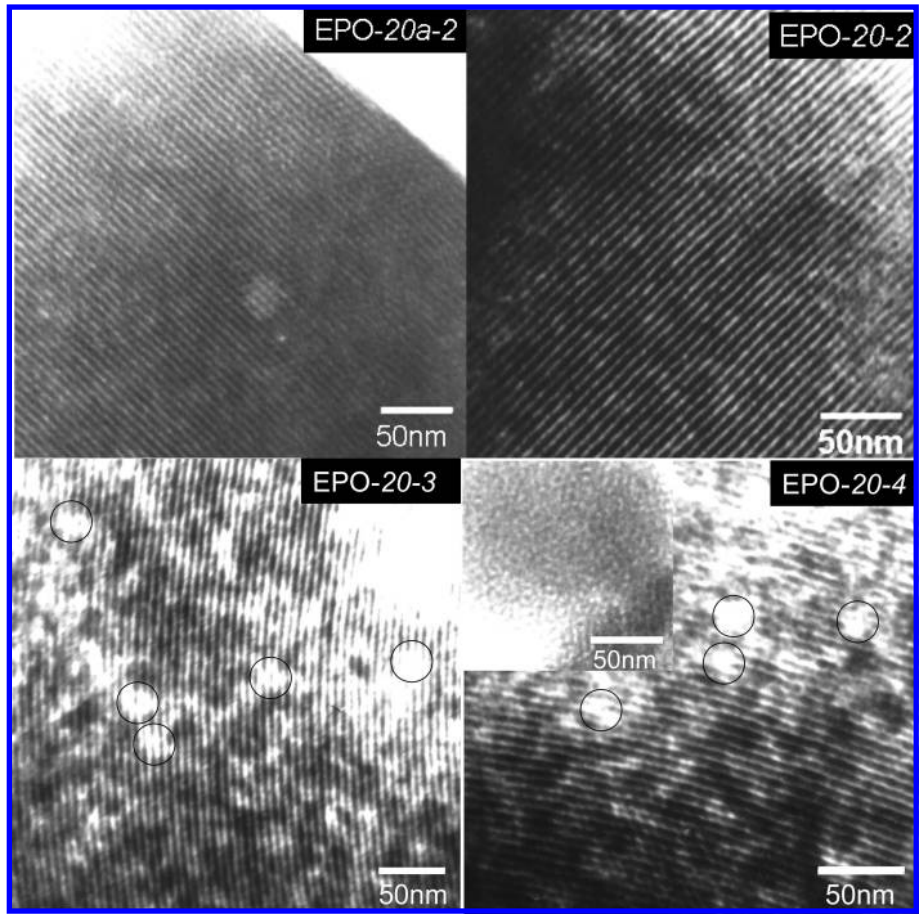

Figure 5. TEM images of phosphonate ester and phosphonic acid functionalized mesoporous organosilicas. Cycles in the image indicates the void defect in the nanochannel.

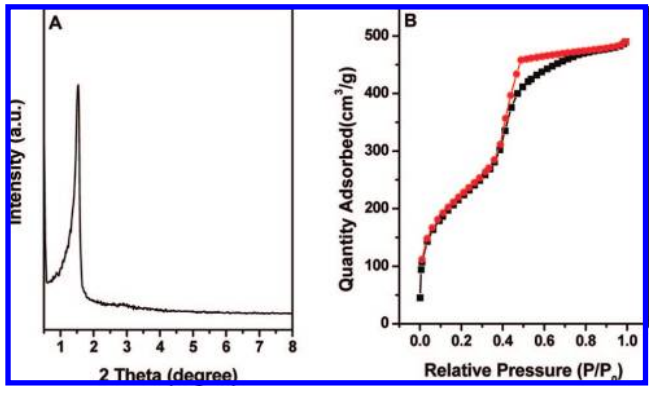

Figure 6. XRD pattern (A) and N_2 sorption isotherm (B) of EPO-20a-2 (surfactant was extracted with ethanol)

favor the formation of highly ordered mesoporous structures. Thus a higher salt concentration decreases the regularity of the mesoporous materials. In addition, the formation of irregularly shaped holes might be related to lower dissolvability of the alcohol burst produced during the fast hydrolysis of silane in the presence of large amounts of NaCl. The real reason for the formation of irregularly shaped holes in the presence of NaCl is not very clear now. But we do believe it is related with the increased hydrolysis and condensation rate of the silane precursor and the perturbation of the double layer potential of organic−inorganic composites by NaCl.[52,53]

Figure 3B displays the nitrogen sorption isotherms of EPO-20-*n* samples. All EPO-20-*n* samples display typical type-IV isotherm patterns with a sharp capillary condensation step at relative pressures (P/P_0) in the range of 0.4−0.5, indicating that these materials have mesopores around 3.2 nm. EPO-20-1 and EPO-20-2 exhibit H2 hystersis loops, similar to EPO-20 synthesized without the addition of NaCl. In addition to the capillary condensation step at $P/P_0 = 0.4-0.5$, EPO-20-3 and EPO-20-4 also possess an uncommon type-H3 hysteresis loop at P/P_0 values between 0.5 and 0.9. The existence of such a type-H3 loop may be due to the existence of irregularly shaped holes in the pore wall of the mesoporous materials, as evidenced by the TEM characterization. EPO-20-1 has a smaller pore diameter than EPO-20, but their BET surface area and pore volume are comparable (Table 1). From EPO-20-1 to EPO-20-4, the BET surface area and pore volume first increase and then decrease and reach a plateau for EPO-20-3 (Table 1).

To investigate the influence of the surfactant extraction method on the structural order of the materials, corresponding mesoporous ethane silica functionalized with phosphonate ester, EPO-20a-2, was synthesized for comparison by extracting the surfactant using ethanol. Figure 6A shows the XRD pattern of EPO-20a-2. Only one sharp diffraction peak was observed in the low 2θ region. The absence of other diffraction peaks shows that the structure of EPO-20a-2 is not as ordered as that of EPO-20-2, which exhibits three diffraction peaks in its XRD pattern. The $d(100)$ spacing of EPO-20-2 is larger than that of EPO-20a-2, implying lattice expansion of the material after HCl treatment. Similar to EPO-20-2, the TEM image of EPO-20a-2 also clearly shows two-dimensional hexagonal arrangement of the mesopore throughout the samples (Figure 5). EPO-20a-2 displays typical type-IV isotherm patterns with a sharp capillary condensation step at relative pressures (P/P_0) in the range of

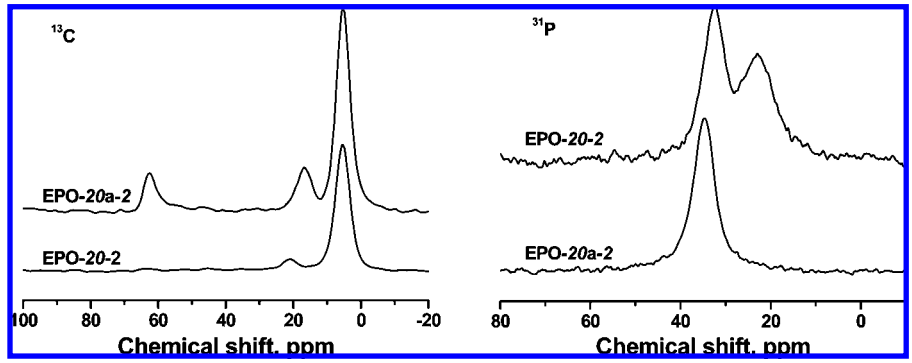

Figure 7. ^{13}C CP MAS NMR and ^{31}P MAS NMR spectra of EPO-20a-2 (surfactant was extracted with ethanol) and EPO-20-2 (as-synthesized sample was treated with concentrated HCl).

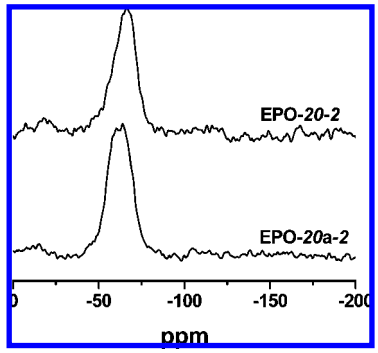

Figure 8. ^{29}Si MAS NMR spectra of EPO-20a-2 (surfactant was extracted with ethanol) and EPO-20-2 (as-synthesized sample was treated with concentrated HCl).

0.4−0.5, indicating that this material has uniform mesopore (Figure 6B). The pore diameter of EPO-20a-2 is smaller than EPO-20-2, which can be due to the existence of large phosphonate in the pore of EPO-20a-2 (Table 1). Other EPO-20a-*n* samples show similar isotherm patterns to the corresponding EPO-20-*n* (Figure S2 of Supporting Information). All of these results reveal that postsynthesis treatment in concentrated HCl can improve the structure order of the materials and only has slight influence on the textural properties of the materials.

3.3. Framework Composition. The framework composition of the representative samples EPO-20a-2 and EPO-20-2 was analyzed by solid-state NMR measurements. ^{13}C CP-MAS NMR spectra of the samples are shown in Figure 7. Three resonances were observed at 5.2, 16.8, and 62.5 ppm for EPO-20a-2. The signal at 5.2 ppm can be assigned to the mixture of carbon species of $-SiCH_2CH_2Si-$[6] and $-SiCH_2CH_2P-$.[54] The resonances at 16.8 and 62.5 ppm represent the phosphonate ester group. The resonance at 16.8 ppm also masks the carbon species of $-SiCH_2CH_2P-$.[54] ^{31}P MAS NMR spectrum of EPO-20a-2 exhibits one signal at 34.6 ppm, which can be assigned to phosphor species of $-P(O)(OCH_2CH_3)_2$ (Figure 7).[37,54] The element analysis of EPO-20a-*n* was also confirmed by the presence of phosphorus (Table S1 of Supporting Information). The ^{29}Si MAS NMR spectrum of EPO-20a-2 exhibits a broad peak centered at −64.0 ppm, which can be assigned to the mixture of silicon species bonded with $-CH_2CH_2P(O)(OCH_2CH_3)_2$ and silicon species bridged by $-CH_2CH_2-$ (Figure 8).[6,54] The NMR results indicate that phosphonic acid diethyl ester group is covalently incorporated into the framework of mesoporous ethane silicas.

Phosphonate ester groups can be transformed readily to phosphonic acid groups by acid-catalyzed hydrolytic dealkylation in concentrated HCl. To generate phosphonic acid groups during template removing process, the as-synthesized EPO-20-2 was treated with concentrated HCl. Two signals were observed in ^{13}C CP-MAS NMR spectrum of EPO-20-2 (Figure 7). The signal at 5.2 ppm can be assigned to the mixture of carbon species of $-SiCH_2CH_2Si-$[6] and $-SiCH_2CH_2P-$.[54] The signal at 21.2 ppm can be assigned to the carbon species of $-SiCH_2CH_2P-$. The disappearance of the signal at 62.5 ppm strongly confirms the successful dealkylation of the ester group. No signals related to the surfactant were observed, indicating the complete removal of template during the dealkylation process. The chemical shift of $PO(OH)_2$ is very close to that of $PO(OC_2H_5)_2$; therefore the signal at 32.3 ppm in ^{31}P MAS NMR spectrum of EPO-20-2 could be assigned to phosphonic acid (Figure 7). The additional signal at 23.0 ppm is due to P species of phosphonic acid which forms hydrogen bond with surface Si-OH groups.[54,55] ^{29}Si NMR spectrum of EPO-20-2 exhibits a broad peak centered at −66.4 ppm (Figure 8). In comparison with the chemical shift of silicon species of EPO-20a-2 (−64.0 ppm), this chemical shift was altered to upfield. The result of ^{29}Si NMR suggests that silicon species undergo further condensation during the surfactant extraction process. The Si−C bond is stable enough to survive the dealkylation process as evidenced by the fact that no signals for $SiO_n(OH)_{4-n}$ species in the range of −90 to −110 ppm were observed in ^{29}Si NMR spectrum of EPO-20-2.

3.4. Potential in Enrichment of Phosphopeptides from a Trypsin Digest of Standard Phosphoprotein. The phosphonic acid functionalized PMOs possess not only the highly ordered mesoporous structure with a high specific surface area but also the abundant phosphonic groups at the inner wall of the mesopores, which make it the potential IMAC adsorbent for the selective capture of phosphopeptides in the analysis of phosphoproteome via the preload of metal ions onto the interior phosphonic groups. To investigate the promising potential of the synthesized phosphonic acid functionalized PMO in the capture of phosphopeptides from the proteolytic digest, EPO-20-2 and EPO-20-3 were used as the IMAC adsorbents in the analysis of standard phosphoprotein of bovine β-casein with five know phosphorylation sites through the preload of metal ions of Zr^{4+} and Fe^{3+} (denoted as Zr^{4+}-EPO-20-*n* and Fe^{3+}-EPO-20-*n*) based on MALDI-TOF MS analysis.[30,31] (The detail description of protein digestion and the preload of metal ions on the IMAC adsorbents can be found in Supporting Information).

The typical capture of phosphopeptides from the tryptic digest of bovine β-casein (1 pmol) was demonstrated by using the Zr^{4+} and Fe^{3+}-loaded EPO-20-*n* ($n = 2, 3$) and analyzed by MALDI-TOF MS. The corresponding MALDI-TOF mass spectra are illustrated in Figure 9, where Figure 9a represents the obtained

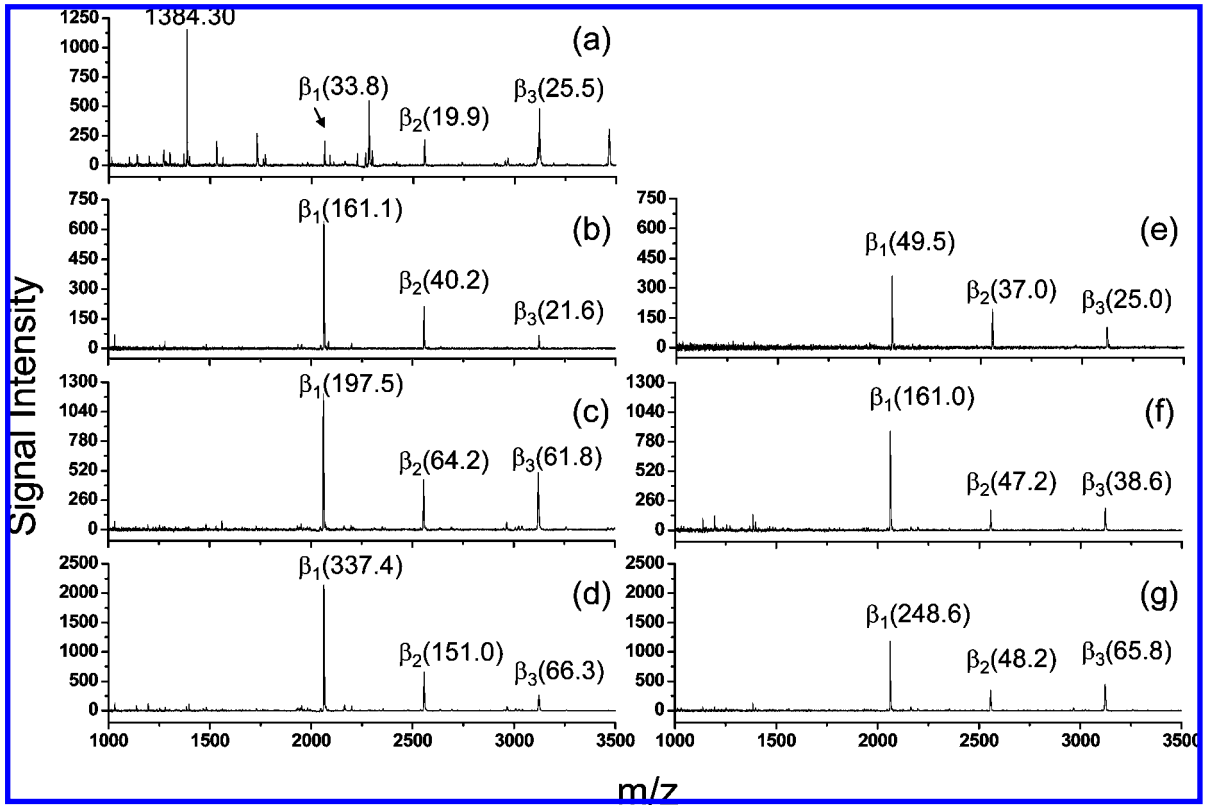

Figure 9. MALDI-TOF mass spectra of tryptic digest of β-casein (a) via direct analysis and after treament by IMAC materials of (b) Zr^{4+}-POROS 20, (c) Zr^{4+}-EPO-20-2, (d) Zr^{4+}-EPO-20-3, (e) Fe^{3+}-POROS 20, (f) Fe^{3+}-EPO-20-2, and (g) Fe^{3+}-EPO-20-3. The numbers in parentheses represent the S/N ratios of the peaks.

mass spectrum via direct analysis without treatment of IMAC materials; parts b−d of Figure 9 represent the MALDI-TOF mass spectra of the same amount of tryptic digest of β-casein treated by Zr^{4+}-loaded IMAC materials, and parts e and f of Figure 9 represent the mass spectra with Fe^{3+}-loaded IMAC materials. As can be seen in Figure 9, the phosphorylated peptides (β_1, β_2, and β_3 with *m/z* of 2061.94, 2556.93, and 3133.56, respectively, with the amino acid sequence described in Table S1 of Supporting Information) and the nonphosphorylated peptides arising from the tryptic digest of β-casein were codetected in the direct MALDI MS analysis manner, while only the phosphorylated peptides were detected after using the Zr^{4+}- and Fe^{3+}-loaded IMAC materials. This was because of the fact that the Zr^{4+}- and Fe^{3+}-loaded IMAC materials could provide the highly selective affinity to the phosphopeptides. In a comparison to the commercially available POROS 20 MC beads that was the most widely utilized IMAC beads for the isolation of phosphopeptides,[31−33,36,56] the peak intensities and the S/N of phosphopeptide peaks of β_1, β_2, and β_3 in parts c, d, f, and g of Figure 9 determined by using EPO-20-*n* ($n = 2, 3$) are all greater than those in parts b and e of Figure 9 by using POROS 20 via the load of cations of either Zr^{4+} or Fe^{3+}. This was not only because of the presence of phosphonic acid groups in the EPO-20-*n* having the stronger coordination capability to metal ions (see Supporting Information) than those of the iminodiacetic acid (IDA) groups provided by the commercial beads[57] but also because the higher surface area and the unique mesoporous structure of EPO-20-*n* made the capture of phosphopeptide on the phosphonic acid functionalized PMOs was much more efficient than that on the commercial POROS-20 beads (Table 1 and Figure S3 of Supporting Information).

The phospho-PMOs could be used as the promising IMAC adsorbents for the enrichment of phosphopeptides via the loading of metal ions. The further systematic investigations on the enrichment and/or selective capture of phosphopeptides from the complex biological samples by using the phosphor-PMOs with different pore structures will be carried out in future for the comprehensive exploration and deep understanding of this kind of material in bioanalysis.

4. Conclusions

Highly ordered mesoporous ethane silicas with phosphonic acid were synthesized by co-condensation of BTME and PETES under acidic medium using Brij-76 as the template. Without the addition of inorganic salt (NaCl), ordered mesoporous structures could be obtained at molar ratio of PETES/(PETES+BTME) less than 10%. The mesosturcture of the material synthesized with high PETES concentration was dramatically improved by adding suitable amounts of an inorganic salt (NaCl). The TEM and N_2 sorption results clearly showed that the higher amounts of NaCl could help the formation of void defects in the pore wall of the mesoporous materials. After immobilization with metal ions (Zr^{4+} and Fe^{3+}), the resultant materials were used as effective IMAC adsorbents for the enrichment of phosphopeptides, which clearly showed the potential of the phosphonic acid-functionalized PMOs with high surface area and the ordered meso-nanopore structure as the promising IMAC adsorbents in the specific capture of phosphopeptides.

Acknowledgment. This work was financially supported by the National Natural Science Foundation of China (20703044, 20423004), National Basic Research Program of China (2005 CB 221407), and Programme Strategic Scientific Alliances between China and The Netherlands (2008DFB50130).

Supporting Information Available: Details about protein digestion, enrichment of phosphopeptides, preload of metal ions on the IMAC adsorbents, N_2 sorption isotherms, and textural properties of phosphonate ester and phosphonic acid functionalized materials. This information is available free of charge via the Internet at http://pubs.acs.org.

References and Notes

(1) Hunter, T. *Cell* **2000**, *100*, 113.
(2) Bennett, K. L.; Stensballe, A.; Podtelejnikov, A. V.; Moniatte, M.; Jensen, O. N. *J. Mass. Spectrom.* **2002**, *37*, 179.
(3) Zhou, H. L.; Watts, J. D.; Aebersold, R. *Nat. Biotechnol.* **2001**, *19*, 375.
(4) Beausoleil, S. A.; Villen, J.; Gerber, S. A.; Rush, J.; Gygi, S. P. *Nat. Biotechnol.* **2006**, *24*, 1285.
(5) Asefa, T.; MacLachan, M. J.; Coombs, N.; Ozin, G. A. *Nature* **1999**, *402*, 867.
(6) Inagaki, S.; Guan, S.; Fukushima, Y.; Ohsuna, T.; Terasaki, O. *J. Am. Chem. Soc.* **1999**, *121*, 9611.
(7) Melde, B. J.; Holland, B. T.; Blanford, C. F.; Stein, A. *Chem. Mater.* **1999**, *11*, 3302.
(8) Sayari, A.; Hamoudi, S. *Chem. Mater.* **2001**, *13*, 3151.
(9) Kickelbick, G. *Angew. Chem., Int. Ed.* **2004**, *43*, 3102.
(10) Hartmann, M. *Chem. Mater.* **2005**, *17*, 4577.
(11) Hatton, B.; Landskron, K.; Whitnall, W.; Perovic, D.; Ozin, G. A. *Acc. Chem. Res.* **2005**, *38*, 305.
(12) Hunks, W. J.; Ozin, G. A. *J. Mater. Chem.* **2005**, *15*, 3716.
(13) Vinu, A.; Hossain, K. Z.; Ariga, K. *J. Nanosci. Nanotechnol.* **2005**, *5*, 347.
(14) Hoffmann, F.; Cornelius, M.; Morell, J.; Froba, M. *Angew. Chem., Int. Ed.* **2006**, *45*, 3216.
(15) Hoffmann, F.; Cornelius, M.; Morell, J.; Froba, M. *J. Nanosci. Nanotechnol.* **2006**, *6*, 265.
(16) Wan, Y.; Zhang, D. Q.; Hao, N.; Zhao, D. Y *Int. J. Nanotechnol.* **2007**, *4*, 66.
(17) Salonen, J.; Kaukonen, A. M.; Hirvonen, J.; Lehto, V. P. *J. Pharm. Sci.* **2008**, *97*, 632.
(18) Zhang, W. H.; Zhang, X. N.; Hua, Z.; Harish, P.; Schroeder, F.; Hermes, S.; Cadenbach, T.; Shi, J. L.; Fischer, R. A. *Chem. Mater.* **2007**, *19*, 2663.
(19) Yang, Q. H.; Liu, J.; Yang, J.; Kapoor, M. P.; Inagaki, S.; Li, C. *J. Catal.* **2004**, *228*, 265.
(20) Yang, Q. H.; Liu, J.; Yang, J.; Zhang, L.; Feng, Z. C.; Zhang, J.; Li, C. *Microporous Mesoporous Mater.* **2005**, *77*, 257.
(21) Yang, Q. H.; Kapoor, M. P.; Inagaki, S. *J. Am. Chem. Soc.* **2002**, *124*, 9694.
(22) Jiang, D. M.; Yang, Q. H.; Wang, H.; Zhu, G. R.; Yang, J.; Li, C. *J. Catal.* **2006**, *239*, 65.
(23) Jiang, D. M.; Gao, J. S.; Yang, J.; Su, W. G.; Yang, Q. H.; Li, C. *Microporous Mesoporous Mater.* **2007**, *105*, 204.
(24) Burleigh, M. C.; Markowitz, M. A.; Spector, M. S.; Gaber, B. P. *J Phys. Chem. B* **2001**, *105*, 9935.
(25) Burleigh, M. C.; Markowitz, M. A.; Spector, M. S.; Gaber, B. P. *Langmuir* **2001**, *17*, 7923.
(26) Burleigh, M. C.; Markowitz, M. A.; Spector, M. S.; Gaber, B. P. *Chem. Mater.* **2001**, *13*, 4760.
(27) Asefa, T.; Kruk, M.; MacLachlan, M. J.; Coombs, N.; Grondey, H.; Jaroniec, M.; Ozin, G. A. *J. Am. Chem. Soc.* **2001**, *123*, 8520.
(28) Guo, W. P.; Park, J. Y.; Oh, M. O.; Jeong, H. W.; Cho, W. J.; Kim, I.; Ha, C. S. *Chem. Mater.* **2003**, *15*, 2295.
(29) Zhu, G. R.; Yang, Q. H.; Jiang, D. M.; Yang, J.; Zhang, L.; Li, Y.; Li, C. *J. Chromatogr. A* **2006**, *1103*, 257.
(30) Stensballe, A.; Andersen, S.; Jensen, O. N. *Proteomics* **2001**, *1*, 207.
(31) Larsen, M. R.; Thingholm, T. E.; Jensen, O. N.; Roepstorff, P.; Jorgensen, T. J. D. *Mol. Cell. Proteomics* **2005**, *4*, 873.
(32) Zhou, H. J.; Xu, S. Y.; Ye, M. L.; Feng, S.; Pan, C. S.; Jiang, X. G.; Li, X.; Han, G. H.; Fu, Y.; Zou, H. F. *J. Proteome. Res.* **2006**, *5*, 2431.
(33) Feng, S.; Ye, M. L.; Zhou, H. J.; Jiang, X. G.; Jiang, X. N.; Zou, H. F.; Gong, B. L. *Mol. Cell. Proteomics* **2007**, *6*, 1656.
(34) Zhao, L.; Wu, R. A.; Han, G. H.; Zhou, H. J.; Ren, L. B.; Tian, R. J.; Zou, H. F. *J. Am. Soc. Mass Spectrom.* **2008**, *19*, 1176.
(35) Imanishi, S. Y.; Kochin, V.; Erikssion, J. E. *Proteomics* **2007**, *7*, 174.
(36) Pan, C. S.; Ye, M. L.; Yu, Y. G.; Feng, S.; Jiang, X. G.; Han, G. H.; Zhu, J. J.; Zou, H. F. *J. Proteome. Res.* **2006**, *5*, 3114.
(37) Yang, Q. H.; Yang, J.; Liu, J.; Li, Y.; Li, C. *Chem. Mater.* **2005**, *17*, 3019.
(38) Zhang, L.; Liu, J.; Yang, J.; Yang, Q. H.; Li, C. *Microporous Mesoporous Mater.* **2008**, *109*, 172.
(39) Sujandi, Park, S. E.; Han, D. S.; Han, S. C.; Jin, M. J.; Ohsuna, T. *Chem. Commun.* **2006**, 4131.
(40) Wang, X. G.; Lin, K. S. K.; Chan, J. C. C.; Cheng, S. *Chem. Commun.* **2004**, 2762.
(41) Chong, A. S. M.; Zhao, X. S. *J. Phys. Chem. B* **2003**, *107*, 12650.
(42) Yu, C. Z.; Tian, B. Z.; Fan, J.; Stucky, G. D.; Zhao, D. Y. *J. Am. Chem. Soc.* **2002**, *124*, 4556.
(43) Guo, W. P.; Kim, I.; Ha, C. S. *Chem. Commun.* **2003**, 2692.
(44) Zhao, L.; Zhu, G. S.; Zhang, D. L.; Di, Y.; Chen, Y.; Terasaki, O.; Qiu, S. L. *J. Phys. Chem. B* **2005**, *109*, 764.
(45) Landskron, K.; Ozin, G. A. *Science* **2004**, *306*, 1529.
(46) Hunks, W. J.; Ozin, G. A. *Chem. Commun.* **2004**, 2426.
(47) Zhang, L.; Yang, Q. H.; Zhang, W. H.; Li, Y.; Yang, J.; Jiang, D. M.; Zhu, G. R.; Li, C. *J. Mater. Chem.* **2005**, *15*, 2562.
(48) Qiao, S. Z.; Yu, C. Z.; Hu, Q. H.; Jin, Y. G.; Zhou, X. F.; Zhao, X. S.; Lu, G. Q. *Microporous Mesoporous Mater.* **2006**, *91*, 59.
(49) Bao, X. Y.; Li, X.; Zhao, X. S. *J. Phys. Chem. B* **2006**, *110*, 2656.
(50) Brinker, C. J.; Scherer, G. W. *Sol-Gel Science: The Physics and Chemistry of Sol-Gel Processing*; Academic Press: San Diego, 1990.
(51) Bagshaw, S. A. *J. Mater. Chem.* **2001**, *11*, 831.
(52) Yu, J.; Shi, J. L.; Chen, H. R.; Yan, J. N.; Yan, D. S. *Microporous Mesoporous Mater.* **2001**, *46*, 153.
(53) Monnier, A.; Schuth, F.; Huo, Q.; Kumar, D.; Margolese, D.; Maxwell, R. S.; Stucky, G. D.; Krishnamurty, M.; Petroff, P.; Firouzi, A.; Janicke, M.; Chmelka, B. F. *Science* **1993**, *261*, 1299.
(54) Aliev, A.; Ou, D. L.; Ormsby, B.; Sullivan, A. *J. Mater. Chem.* **2000**, *10*, 2758.
(55) Corriu, R. J. P.; Datas, L.; Guari, Y.; Mehdi, A.; Reye, C.; Thieuleux, C. *Chem. Commun.* **2001**, 763.
(56) Zhou, H. J.; Tian, R. J.; Ye, M. L.; Xu, S. Y.; Feng, S.; Pan, C. S.; Jiang, X. G.; Li, X.; Zou, H. F. *Electrophoresis* **2007**, *28*, 2201.
(57) Stanghellini, P. L.; Boccaleri, E.; Diana, E.; Alberti, G.; Vivani, R. *Inorg. Chem.* **2004**, *43*, 5698.

JP8093534